PERGAMON

International Journal of Solids and Structures 37 (2000) 6825–6842

INTERNATIONAL JOURNAL OF SOLIDS and STRUCTURES

www.elsevier.com/locate/ijsolstr

Buckling localization in a cylindrical panel under axial compression

Viggo Tvergaard [a], Alan Needleman [b,*]

[a] *Department of Solid Mechanics, Technical University of Denmark, DK-2800 Lyngby, Denmark*
[b] *Division of Engineering, Brown University, Providence, RI 02912, USA*

Received 10 November 1999

Abstract

Localization of an initially periodic buckling pattern is investigated for an axially compressed elastic–plastic cylindrical panel of the type occurring between axial stiffeners on cylindrical shells. The phenomenon of buckling localization and its analogy with plastic flow localization in tensile test specimens is discussed in general. For the cylindrical panel, it is shown that buckling localization develops shortly after a maximum load has been attained, and this occurs for a purely elastic panel as well as for elastic–plastic panels. In a case where localization occurs after a load maximum, but where subsequently the load starts to increase again, it is found that near the local load minimum, the buckling pattern switches back to a periodic type of pattern. The inelastic material behavior of the panel is described in terms of J_2 corner theory, which avoids the sometimes unrealistically high buckling loads predicted by the simplest flow theory of plasticity.

Keywords: Buckling localization; Cylindrical panel; Axial compression

1. Introduction

Localization, in the sense of a more or less abrupt change from a smoothly varying deformation pattern to a pattern involving one or more regions of highly localized deformation, occurs in a wide variety of circumstances, including shear band localizations in structural metals, rocks and concrete, and localized tearing in sheet forming operations. The onset of necking in the round bar tensile test is a classic example of this type of localization. Considére (1885) showed that necking initiates at the maximum load point, at least for the case of a long thin bar (Hutchinson and Miles, 1974).

A similar observation in structural buckling is that the final buckled configuration is a localized mode in contrast to the periodic mode associated with the critical buckling load. The experiments of Moxham (1971) show that the final collapse mode of an axially compressed steel plate strip involves one buckle rather than a periodic pattern. That the basic mechanism of buckling localization is associated with a bifurcation

* Corresponding author. Tel.: +1-401-863-2863; fax: +1-401-863-1157.
E-mail address: needle@engin.brown.edu (A. Needleman).

0020-7683/00/$ - see front matter
PII: S0020-7683(99)00316-9

in the vicinity of the maximum load point – in close analogy with the Considére (1885) treatment of tensile necking – was pointed out by Tvergaard and Needleman (1980).

A bifurcation into a localized mode at, or subsequent to, the attainment of a load maximum is key to the understanding of a variety of buckling phenomena. Examples include the transition from a diamond mode collapse pattern for thin axially compressed circular cylindrical shells to an axisymmetric collapse mode for thick shells; the buckling of railroad tracks induced by constrained thermal expansion of the rails and the localized collapse of tubes subject to bending.

Relatively thick axially compressed circular cylindrical shells collapse axisymmetrically, while thinner shells buckle in a diamond pattern. In all cases, the initial buckling mode for elastic–plastic circular cylindrical shells is axisymmetric. In the plastic range, the critical stress for non-axisymmetric modes is slightly higher than the critical stress for the axisymmetric mode. For thicker shells, bifurcation into a non-axisymmetric mode occurs after a load maximum has been attained (Gellin, 1979; Tvergaard, 1983a). Localization following the load maximum for thicker shells is what precludes the non-axisymmetric bifurcation and causes collapse to occur in an axisymmetric mode (Tvergaard, 1983b; Mikkelsen, 1995).

Railroad tracks buckle due to thermally induced compressive forces. The railroad track can be modeled as a beam, representing the rails and cross-ties, on a softening foundation that represents the underlying crushed stone layer. Using representative values for parameters, the critical temperature rise for the critical buckling mode, which is a short wavelength periodic mode, is 600°C (Tvergaard and Needleman, 1981). When account is taken of small imperfections, a maximum compressive force is usually attained, which then leads to buckling mode localization. The maximum temperature rise with realistic imperfections is $\approx$60°C (Tvergaard and Needleman, 1981).

A maximum moment is reached for a tube subject to bending, mainly due to ovalization of the cross-section (the Brazier effect), with possible plastic yielding or buckling into a short wavelength pattern on the compressed side of the tube, further decreasing the bending stiffness. Tube collapse then takes place in a localized mode (Tvergaard and Needleman, 1980; Kyriakides and Ju, 1992; Ju and Kyriakides, 1992). Localized buckling also occurs under dynamic loading conditions and is of interest in connection with the response of shock-absorbing devices. Results on the effect of inertia on the tendency for buckling pattern localization and the effect this has on the energy absorbed during buckling are shown in Tvergaard and Needleman (1983).

Narrow cylindrical panels occur in stiffened cylindrical shells and, depending on their curvature, may or may not have a load maximum associated with deformation in the periodic buckling mode. On the basis of his general theory of elastic stability (Koiter, 1945), it has been shown by Koiter (1956) that sufficiently flat elastic cylindrical panels subject to axial compression have a stable initial post-buckling response, and so do not attain a load maximum in the vicinity of the bifurcation point. For more curved panels, the initial post-buckling response is unstable so that a load maximum is attained in the vicinity of the bifurcation point and the structure is imperfection sensitive. Tvergaard (1977) analyzed the post-buckling behavior and imperfection sensitivity of elastic–plastic cylindrical panels. The decrease in stiffness associated with plastic yielding increased the range of panel curvatures that give rise to imperfection sensitive response. Thus, whether or not a cylindrical panel is prone to localization depends on the panel curvature and, for elastic-plastic panels, on the strain hardening characteristics of the material.

In this article, we analyze the development of buckling pattern localization in elastic–plastic cylindrical panels subject to axial compression. Two models that illustrate the main features of buckling pattern localization are reviewed; a simple one-dimensional model and a beam on a softening foundation. The models show, in simple contexts, the association between a load maximum and buckling mode localization. For the cylindrical panel, both cases where bifurcation into the periodic mode occurs after plastic yielding as well as cases, where bifurcation occurs in the elastic range are considered. The effects of various types of imperfections are analyzed. In all cases, the association between a load maximum and localization is maintained.

2. Models for localization

2.1. One-dimensional model

The localization of buckling patterns is analogous to the necking of tensile bars. A simple one-dimensional model, Tvergaard and Needleman (1980), illustrated the basic mechanism involved. Consider a homogeneous axially compressed bar constrained to remain straight, which can be regarded as a one-dimensional model of a periodically buckled structure. The axial force is taken to be a nonlinear function of the axial strain. The effects of both geometric and material nonlinearities are incorporated into the force–strain response of the bar.

For a bar of length L, the end displacements are prescribed at $x = 0, L$. The incremental relation between the axial force N and the strain ϵ is

$$\dot{N} = K\dot{\epsilon}, \quad \dot{\epsilon} = \dot{u}_{,x}, \tag{2.1}$$

where $(\,)_{,x}$ denotes differentiation with respect to the axial coordinate x and $(\dot{\ })$ denotes incremental quantities.

Incremental equilibrium requires that

$$\dot{N}_{,x} = 0. \tag{2.2}$$

At any stage of loading, one possible solution is continued homogeneous deformation. The possibility of a bifurcation from the homogeneous state is sought, where the bifurcation mode consists of a localized region that can undergo incremental straining different from that in the bulk, although each region itself deforms homogeneously.

Incremental equilibrium requires

$$\dot{N}_{\mathrm{A}} = \dot{N}_{\mathrm{B}}, \tag{2.3}$$

where the subscripts A and B denote quantities outside and inside the localized region, respectively.

Since,

$$\dot{N}_{\mathrm{A}} = K\dot{\epsilon}_{\mathrm{A}}, \quad \dot{N}_{\mathrm{B}} = K\dot{\epsilon}_{\mathrm{B}} \tag{2.4}$$

incremental equilibrium implies

$$K(\dot{\epsilon}_{\mathrm{A}} - \dot{\epsilon}_{\mathrm{B}}) = 0. \tag{2.5}$$

Hence, the onset of localization is only possible at the maximum load point, i.e. when $K = 0$.

The post-localization response can be determined within the context of this bar model. Let L_{A} and L_{B} denote the lengths associated with regions A and B, respectively. Then,

$$L = L_{\mathrm{A}} + L_{\mathrm{B}}. \tag{2.6}$$

Since $\epsilon = \Delta u/\Delta x$,

$$\dot{\epsilon} = (1 - \rho)\dot{\epsilon}_{\mathrm{A}} + \rho\dot{\epsilon}_{\mathrm{B}}, \tag{2.7}$$

where $\rho = L_{\mathrm{B}}/L$.

Eqs. (2.7) and (2.3) combine to give

$$\dot{\epsilon} = \frac{\dot{N}}{K_{\mathrm{B}}}\left[\rho + (1 - \rho)\frac{K_{\mathrm{B}}}{K_{\mathrm{A}}}\right]. \tag{2.8}$$

At localization $K_{\mathrm{B}} = 0$, while K_{B} is negative after the maximum load. With K_{A} algebraically larger than K_{B}, the post-localization traction–deformation gradient curve lies below the one for homogeneous straining

and, the smaller ρ is, the more quickly the load drops. Hence, the post-localization stiffness depends on the size scale of the localized region and this length scale is set by factors outside the scope of the one-dimensional analysis. For localized buckling in structures, the softening comes from geometric effects, which set the size scale.

For tensile necking (where the sign of N is reversed), a full three-dimensional theory shows that the size of the necked region in a tensile bar is set by the lateral dimensions of the bar (Hutchinson and Miles, 1974). These equations also provide a one-dimensional model for shear band development (Needleman, 1988). However, for shear bands there is no larger geometrical context to provide the length scale. The length scale must be incorporated, implicitly or explicitly, into the material description, or the formulation of the boundary value problem needs to be changed to include a length scale.

In structural buckling, the maximum load may be reached because of nonlinear geometric effects or because of nonlinear material behavior. Whatever the cause, there is a strong tendency for localization when a load maximum is reached so that the simple model has bearing on a variety of buckling problems including, for example, the axially compressed plate strips of Moxham (1971), stiffened panels, bent tubes that reach a maximum load due to the Brazier effect (ovalization of the cross-section) and the axially compressed cylindrical shells analyzed here.

2.2. Beam on a softening foundation

A simple structural model that illustrates the delay between the maximum load point and point of bifurcation leading to localization is a linear elastic beam of length $L\,(0 \leqslant X \leqslant L)$, having bending stiffness EI and subjected to an axial load P. The beam rests on a foundation that provides a restoring force per unit length F.

In the presence of an imperfection $\overline{W}$, the governing equation is

$$EI\frac{\mathrm{d}^4 W}{\mathrm{d}X^4} + P\frac{\mathrm{d}^2 W}{\mathrm{d}X^2} + F = -P\frac{\mathrm{d}^2 \overline{W}}{\mathrm{d}X^2}, \tag{2.9}$$

where $W(X)$ is the lateral deflection in addition to the initial deviation from the straight configuration measured by $\overline{W}(X)$.

The beam is taken to be simply supported, so that the boundary conditions are

$$W = 0, \quad \frac{\mathrm{d}^2 W}{\mathrm{d}X^2} = 0 \quad \text{on } X = 0, L. \tag{2.10}$$

The restoring force is taken to have the bilinear form

$$F = \begin{cases} K_1 W & \text{for} \quad |W| \leqslant W_0, \\ \pm K_1 W_0 + K_2(W \mp W_0) & \text{for} \quad |W| > W_0, \end{cases} \tag{2.11}$$

where the upper sign is used for $W > 0$ and the lower sign for $W < 0$. Attention is focused on softening relations for which $K_2 < K_1$.

For a perfect beam ($\overline{W} \equiv 0$) and restricting attention to beams for which $(K_1/EI)^{1/4}L = n\pi$, for some integer n, the lowest bifurcation load is given by

$$P_{\mathrm{c}} = 2(K_1 EI)^{1/2} \tag{2.12}$$

with the bifurcation mode

$$W_{\mathrm{c}}(X) = \sin\left(\frac{n\pi X}{L}\right). \tag{2.13}$$

An analytical solution can also be obtained for the periodic mode of the imperfect beam (Tvergaard and Needleman, 1980). Bifurcation from the periodic mode can then be investigated numerically. Results from Tvergaard and Needleman (1980) are presented in Fig. 1 for imperfections in the form of the critical mode Eq. (2.13) using the nondimensional quantities

$$w = \frac{W}{W_0}, \quad \delta = \frac{\overline{W}}{W_0}, \tag{2.14}$$

$$\beta = \frac{K_2}{K_1}, \quad \lambda = \frac{P}{2(K_1 EI)^{1/2}}. \tag{2.15}$$

In Fig. 1, $\beta = 0.1$ and the dotted line shows the limiting value of the load as $w_m \to \infty$, where w_m is the lateral deflection amplitude. In the periodic mode, the load versus lateral deflection response is independent of the length of the beam. The arrows mark, where bifurcation takes place for various values of $n = (K_1/EI)^{1/4} L/\pi$. The bifurcation modes are constrained to be symmetrical about the center of the beam. As the length of the beam increases, the bifurcation point approaches the maximum load point, which is the bifurcation point according to the one-dimensional model in Section 2.1.

In Needleman and Tvergaard (1982), a full numerical solution, including the post-localization response, was carried out for an imperfection given by

$$W = W_0 \left[\delta_1 \sin \frac{m\pi X}{L} - \delta_2 \sin \frac{(m-2)\pi X}{L} \right]. \tag{2.16}$$

Fig. 2 shows the resulting curves of load versus average axial strain ϵ for $\beta = 0.1$, $\delta_1 = 0.5$ and $m = 9$. With $\delta_2 = 0$, bifurcation into a localized mode occurs just beyond the maximum load point. With $\delta_2 = 0.025$, the buckling pattern remains nearly periodic until around the bifurcation point, and the

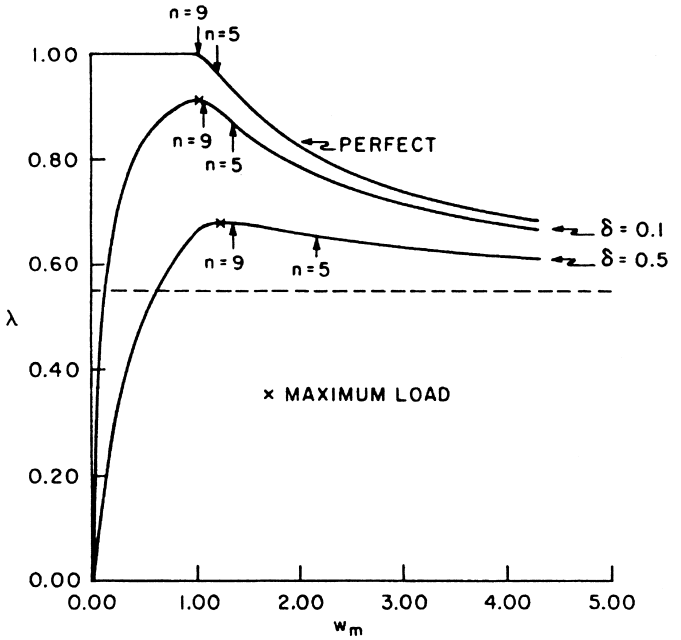

Fig. 1. Load versus lateral deflection amplitude for a column on a softening foundation with $\beta = 0.1$ (Tvergaard and Needleman, 1980).

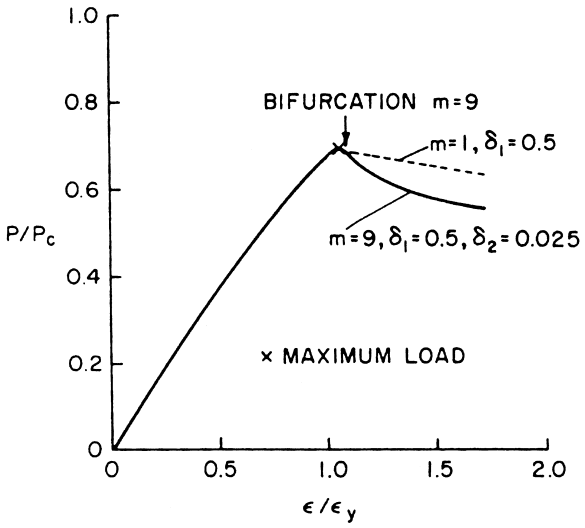

Fig. 2. Load versus average axial strain for an elastic column on an elastic–plastic foundation with $K_2/K_1 = 0.1$ (Needleman and Tvergaard, 1982).

maximum load is nearly the same as for the case with $\delta_2 = 0$. Near the bifurcation point, the buckles near the center of the beam start to grow rapidly while those away from the center start to decay. The buckling pattern at the maximum load point and the localized buckling pattern that develops subsequently are shown in Fig. 3. The "width" of the localized region in Fig. 3 is set by the geometry of the structure. In these calculations, the restoring force relation is taken to be elastic–plastic in that the stiffness K_1 is used in Eq. (2.10), whenever $\dot{W}W < 0$.

The elastic beam on a softening foundation illustrates the characteristic features of buckling pattern localization. The basic mechanism involves a bifurcation, subsequent to the maximum load point, from an initial periodic buckling pattern. The final collapse mode, as illustrated in Fig. 3, bears no resemblance to the deformation pattern prevailing at the maximum load point. Nevertheless, it is the pre-localization deformation pattern that determines the maximum load point.

3. Formulation of cylindrical panel problem

The axially compressed cylindrical panels to be analyzed here are taken to be part of a longitudinally stiffened cylindrical shell. The cylindrical panel occurs as a section of the shell bounded by two neighboring stiffeners, and the local buckling mode of interest is one in which the stiffeners remain straight, while the shell buckles in a short wave pattern between the stiffeners. The initial elastic post-buckling behavior of such panels was analyzed by Koiter (1956), and it was shown that the post-buckling behavior is stable for sufficiently flat panels, as for elastic plates, but unstable for more curved panels. A similar transition from plate-like behavior, for rather flat panels to more unstable behavior for curved panels has been found by Tvergaard (1977) for elastic–plastic cylindrical panels. In the present investigation with focus on buckling localization, we are mainly interested in cases where the primary periodic buckling pattern is characterized by an unstable post-buckling behavior.

The shell has thickness h, radius R, and the circumferential distance between the equally spaced stiffeners is b (Fig. 4). The main effect of the stiffeners is to prevent waviness of radial deflections along their lines of

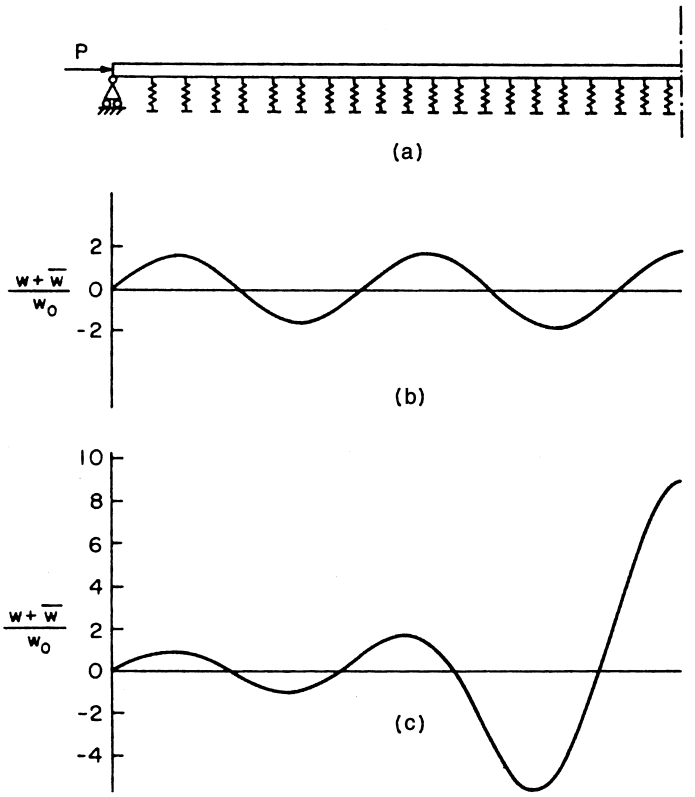

Fig. 3. (a) Elastic column on an elastic–plastic foundation with $K_2/K_1 = 0.1$. (b) Buckling pattern at the maximum load, $\epsilon/\epsilon_y = 1.07$. (c) Buckling pattern after maximum load, at $\epsilon/\epsilon_y = 1.72$ (Needleman and Tvergaard, 1982).

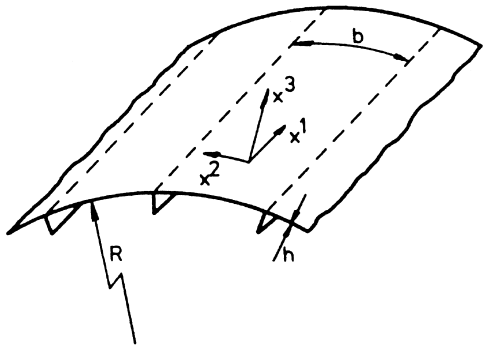

Fig. 4. Part of axially stiffened circular cylindrical shell, showing the cylindrical panels between stiffeners.

attachment. As in Koiter's (1956) analysis of the elastic cylindrical panel, this is the only stiffener constraint accounted for in the present investigation. Thus, it is assumed that there is no constraint on tangential shell displacements along the stiffeners, and that the torsional rigidity of the stiffeners can be neglected.

On the middle surface of the circular cylindrical shell, a point is identified by the coordinates x^1 and x^2, where x^1 measures the distance along the cylinder axis and x^2 measures distance in the circumferential

direction. The displacement components are denoted u^α on the surface base vectors and w on the outward surface normal. The strain measures used are the nonlinear membrane strain tensor

$$\epsilon_{\alpha\beta} = \tfrac{1}{2}\big(u_{\alpha,\beta} + u_{\beta,\alpha}\big) - d_{\alpha\beta}w + \tfrac{1}{2}a^{\gamma\delta}(u_{\gamma,\alpha} - d_{\gamma\alpha}w)(u_{\delta,\beta} - d_{\delta\beta}w) + \tfrac{1}{2}(w_{,\alpha} + d^\gamma_\alpha u_\gamma)(w_{,\beta} + d^\delta_\beta u_\delta) \tag{3.1}$$

and the linear bending strain tensor specified by Koiter (1966)

$$\kappa_{\alpha\beta} = \tfrac{1}{2}\left[\big(w_{,\alpha} + d^\gamma_\alpha u_\gamma\big)_{,\beta} + \Big(w_{,\beta} + d^\gamma_\beta u_\gamma\Big)_{,\alpha} - \tfrac{1}{2}d^\gamma_\alpha\big(u_{\beta,\gamma} - u_{\gamma,\beta}\big) - \tfrac{1}{2}d^\gamma_\beta\big(u_{\alpha,\gamma} - u_{\gamma,\alpha}\big)\right], \tag{3.2}$$

where $a_{\alpha\beta}$ and $d_{\alpha\beta}$ are the metric tensor and the curvature tensor, respectively, of the undeformed middle surface, and $(\ )_{,\alpha}$ denotes covariant differentiation. Greek indices range from 1 to 2, while Latin indices (to be employed subsequently) range from 1 to 3, and the summation convention is adopted for repeated indices. It is noted that strain measures proposed by Niordson (1985) are identical with Eqs. (3.1) and (3.2), except for small differences in the bending strain measure of the order of $d^\gamma_\alpha\epsilon_{\gamma\beta}$.

The three-dimensional constitutive relations are taken to be of the form

$$\dot{\sigma}^{ij} = L^{ijkl}\dot{\eta}_{kl}, \tag{3.3}$$

where σ^{ij} is the stress tensor, η_{kl} is the strain tensor, L^{ijkl} are the instantaneous moduli, and $(\dot{\ })$ denotes an incremental quantity. Since the stress state in the shell is approximately plane, only the in-plane stresses enter into Eq. (3.3). Thus, the constitutive relations can be written as

$$\dot{\sigma}^{\alpha\beta} = \hat{L}^{\alpha\beta\gamma\delta}\dot{\eta}_{\gamma\delta}, \qquad \hat{L}^{\alpha\beta\gamma\delta} = L^{\alpha\beta\gamma\delta} - \frac{L^{\alpha\beta33}L^{33\gamma\delta}}{L^{3333}}. \tag{3.4}$$

The in-plane components of the Lagrangian strain tensor at a distance x^3 outward from the shell middle surface are approximated by

$$\eta_{\alpha\beta} = \epsilon_{\alpha\beta} - x^3\kappa_{\alpha\beta}. \tag{3.5}$$

The membrane stress tensor $N^{\alpha\beta}$ and the moment tensor $M^{\alpha\beta}$ in a shell with thickness h are taken to be

$$N^{\alpha\beta} = \int_{-h/2}^{h/2}\sigma^{\alpha\beta}\,\mathrm{d}x^3, \qquad M^{\alpha\beta} = -\int_{-h/2}^{h/2}\sigma^{\alpha\beta}x^3\,\mathrm{d}x^3. \tag{3.6}$$

Then, from Eqs. (3.4)–(3.6), incremental relations are obtained for $\dot{N}^{\alpha\beta}$ and $\dot{M}^{\alpha\beta}$ in terms of $\dot{\epsilon}_{\gamma\delta}$ and $\dot{\kappa}_{\gamma\delta}$. The requirement of equilibrium is specified in terms of the principle of virtual work.

$$\int_A \{N^{\alpha\beta}\,\delta\epsilon_{\alpha\beta} + M^{\alpha\beta}\,\delta\kappa_{\alpha\beta}\}\mathrm{d}A = P\,\delta U, \tag{3.7}$$

where A is the middle surface area, P is the total axial load acting on the cylinder, U is the axial displacement at one end $(x^1 = a)$, while at the other cylinder end zero axial displacement is prescribed.

As the buckling pattern is periodic in the circumferential direction, due to the constant stiffener spacing, only a shell section between the centers $x^2 = 0, b$ of the two neighboring cylindrical panels needs to be considered. Due to the symmetry of mode displacements about these panel centers, the boundary conditions can be specified as

$$\frac{\partial u_1}{\partial x^2} = u_2 = \frac{\partial w}{\partial x^2} = \frac{\partial^3 w}{\partial (x^2)^3} = 0 \quad \text{at } x^2 = 0, b. \tag{3.8}$$

Across the line of attachment of a stiffener continuity of all field quantities is required, except for the possible discontinuity of the transverse shear force resulting from the constraint

$$\frac{\partial w}{\partial x^1} = 0 \quad \text{at } x^2 = b/2. \tag{3.9}$$

The length of the shell section analyzed is denoted by a, and the symmetric boundary conditions at the two ends are specified as

$$u_1 = 0, \quad \frac{\partial u_2}{\partial x^1} = \frac{\partial w}{\partial x^1} = \frac{\partial^3 w}{\partial (x^1)^3} = 0 \quad \text{at } x^1 = 0, \tag{3.10}$$

$$u_1 = -U, \quad \frac{\partial u_2}{\partial x^1} = \frac{\partial w}{\partial x^1} = \frac{\partial^3 w}{\partial (x^1)^3} = 0 \quad \text{at } x^1 = a \tag{3.11}$$

so that $-U/a = \epsilon_{\text{av}}$ is the specified average strain in the axial direction.

The uniaxial stress–strain curve is represented by a piecewise power law with continuous tangent modulus,

$$\epsilon = \begin{cases} \frac{\sigma}{E} & \text{for } \sigma \leqslant \sigma_{\text{y}}, \\ \frac{\sigma_{\text{y}}}{E}\left[\frac{1}{n}\left(\frac{\sigma}{\sigma_{\text{y}}}\right)^n - \frac{1}{n} + 1\right] & \text{for } \sigma > \sigma_{\text{y}}, \end{cases} \tag{3.12}$$

where n is the strain hardening exponent.

It has been known for half a century that bifurcation calculations based on the simplest deformation theory of plasticity give better agreement with experimentally obtained buckling loads than do similar calculations based on the simplest flow theory. Already, Batdorf (1949) realized that the bifurcation predictions of deformation theory could be rigorously justified by appealing to a more sophisticated flow theory with a vertex on the yield surface. A comprehensive discussion of this "plastic buckling paradox" has been given by Hutchinson (1974).

To account for such effects, the present analyses assume that the elastic–plastic shell material develops a vertex on subsequent yield surfaces, as described by the J_2 corner theory proposed by Christoffersen and Hutchinson (1979). In this theory, the instantaneous moduli for nearly proportional loading are chosen equal to the J_2 deformation theory moduli and for increasing deviation from proportional loading the moduli increase smoothly until they coincide with the elastic moduli for stress increments directed along, or within, the corner of the yield surface.

With M^0_{ijkl} denoting the deformation theory compliances, $\dot{\eta}_{ij} = M^0_{ijkl}\dot{\sigma}^{kl}$, and $\mathscr{M}_{ijkl}$ denoting the linear elastic compliances, the plastic part of the compliances is $C_{ijkl} = M^0_{ijkl} - \mathscr{M}_{ijkl}$. The yield surface in the neighborhood of the current loading point is taken to be a cone in stress deviator space with the cone axis in the direction

$$\lambda^{ij} = s^{ij}\left(C_{mnpq}s^{mn}s^{pq}\right)^{-1/2}. \tag{3.13}$$

Here, $s^{ij} = \sigma^{ij} - g^{ij}\sigma^k_k/3$ is the stress deviator tensor and g_{ij} is the metric tensor in 3-dimensional coordinates. The positive angular measure ϕ of the stress-rate direction relative to the cone axis is defined by

$$\cos\phi = C_{ijkl}\lambda^{ij}\dot{s}^{kl}\left(C_{mnpq}\dot{s}^{mn}\dot{s}^{pq}\right)^{-1/2} \tag{3.14}$$

and a stress-rate potential at the vertex is formulated as

$$W = \tfrac{1}{2}\mathscr{M}_{ijkl}\dot{\sigma}^{ij}\dot{\sigma}^{kl} + \tfrac{1}{2}f(\phi)C_{ijkl}\dot{\sigma}^{ij}\dot{\sigma}^{kl}. \tag{3.15}$$

From this potential the strain rate is obtained as

$$\dot{\eta}_{ij} = \frac{\partial^2 W}{\partial \dot{\sigma}^{ij} \partial \dot{\sigma}^{kl}} \dot{\sigma}^{kl} = M_{ijkl}(\phi)\dot{\sigma}^{kl} \tag{3.16}$$

with ϕ dependent compliances. Since the stress state in the shell is approximately plane, the in – plane stresses enter into Eq. (3.16), which is inverted to yield the plane stress incremental constitutive relations of the form

$$\dot{\sigma}^{\alpha\beta} = \hat{L}^{\alpha\beta\gamma\delta}(\phi)\dot{\eta}_{\gamma\delta}. \tag{3.17}$$

The angle of the yield surface cone is specified by ϕ_c, so that the transition function $f(\phi)$ in Eq. (3.13) is zero for $\phi_c < \phi \leqslant \pi$. In the total loading range, $0 \leqslant \phi \leqslant \phi_0$, $f(\phi)$ is unity, and in the transition region, $\phi_0 \leqslant \phi \leqslant \phi_c$, $f(\phi)$ is chosen to smoothly merge the deformation theory moduli with the elastic moduli in a way which ensures convexity of the incremental relation.

More detailed descriptions of the J_2 corner theory formulations in connection with buckling analyses have been given previously (Needleman and Tvergaard, 1982; Tvergaard, 1983a) and shall not be repeated here. Most analyses in the present paper assume a totally nonlinear material response, $\phi_0 = 0$, and a rather blunt vertex specified by $(\beta_c)_{max} = 100°$, where $\cos\beta = \dot{\sigma}_e\left(3\dot{s}_{ij}\dot{s}^{ij}/2\right)^{-1/2}$ in terms of the Mises effective stress $\sigma_e = (3s_{ij}s^{ij}/2)^{1/2}$.

For an elastic cylindrical panel, Koiter (1956) found the following expression for the critical bifurcation stress

$$\sigma_c = -E\frac{\pi^2 h^2}{3(1-\nu^2)b^2}\left(1+\theta^4\right), \qquad \theta = \frac{\sqrt[4]{[12(1-\nu^2)]}}{2\pi}\frac{b}{\sqrt{(Rh)}} \tag{3.18}$$

valid when $\theta \leqslant 1$ with the axial half wavelength equal to the panel width b. In the following, the parameter θ will be referred to as the panel curvature parameter. For $\theta > 1$, two axial wavelengths are critical simultaneously. A number of cylindrical panels to be considered here are taken to have $h/b = 0.025$, $\sigma_y/E = 0.002$ and $\nu = 0.3$ so that the elastic bifurcation stress (3.18) exceeds the initial yield stress. For these cases, the elastic–plastic bifurcation stress and the corresponding axial wavelength are determined by the use of expressions specified in Tvergaard (1977).

Numerical solutions of the incremental equilibrium equations are obtained by dividing the shell segment analyzed into 24×4 rectangular conforming finite elements. Within an element, each displacement component is approximated by products of Hermitian cubics in the x^1- and x^2-directions, and integrals over the middle surface are evaluated by 4×4 point Gaussian quadrature, with 7 point Simpson integration through the thickness.

As long as the average axial shortening increases monotonically, the end displacement can be prescribed. However, after a load maximum, it is possible for the average axial strain rate to change sign. In such cases, a special additional Rayleigh–Ritz procedure is used to prescribe a normal displacement increment instead of the end displacement (Tvergaard, 1976).

4. Cylindrical panel results

To study the possibility of buckling localization, cylindrical panels with an initial imperfection are analyzed, where the imperfection is specified as an initial normal deflection of the form

$$\overline{w}(x^1, x^2) = \left(\overline{\xi} + \overline{\xi}_1 \cos\frac{\pi x^1}{a}\right) h \cos\frac{m\pi x^1}{a}\cos\frac{\pi x^2}{b}. \tag{4.1}$$

Here, $\overline{\xi}$ is the amplitude of an initial periodic imperfection, and the additional amplitude $\overline{\xi}_1$ specifies a small deviation from periodicity that makes the imperfection slightly larger near $x^1 = 0$ than near $x^1 = a$.

For all the cases to be analyzed here, we take $\overline{\xi}_1/\overline{\xi} = 0.01$. The length of the shell section to be analyzed is in each case taken to be, $a = mb/\alpha$, where the axial wavelength parameter α is calculated so that the imperfection wavelength in the axial direction agrees with the wavelength of the critical bifurcation mode in an infinitely long panel, according to J_2 deformation theory.

In the first case analyzed, the material parameters are $\sigma_y/E = 0.002, v = 0.3$ and $n = 10$, with $(\beta_c)_{max} = 100°$ and $\phi_0 = 0°$ in the J_2 corner theory description. The shell thickness to panel-width ratio is taken to be $h/b = 0.025$ and ratio of the panel width to cylinder radius, b/R, is specified by taking $\theta = 0.6$ in Eq. (3.18). Then, according to Tvergaard (1977), this is a case where an unstable post-buckling behavior is expected to lead to buckling localization. The number of half-waves in the axial direction is taken to be $m = 6$ in (Eq. 4.1), and a bifurcation analysis following expressions specified in Tvergaard (1977) shows that for J_2 deformation theory the critical bifurcation stress and the corresponding axial wavelength are specified by $\sigma_c/E = -0.002220$ and $\alpha = 1.125$.

Fig. 5 shows the average axial compressive stress, σ_{av}, normalized by the bifurcation stress vs. the average axial strain, for three different levels of initial imperfections. For the two smallest imperfection amplitudes, $\overline{\xi} = 0.01$ and $\overline{\xi} = 0.1$, a maximum load is reached, with a rather steep load decay after the maximum for the smallest imperfection. However, for the largest imperfection analyzed, $\overline{\xi} = 1.0$, no maximum is reached in the range analyzed. Therefore, based on the simple localization model, discussed in Section 2, we expect that the buckling pattern will localize for the two smaller imperfection levels, but will not localize for the larger imperfection level, and this is exactly the result obtained here. If load were the prescribed quantity, equilibrium paths beyond the load maximum would be unstable. However, when axial shortening is prescribed, the response remains stable after the load maximum, unless the axial shortening also decreases along the equilibrium path.

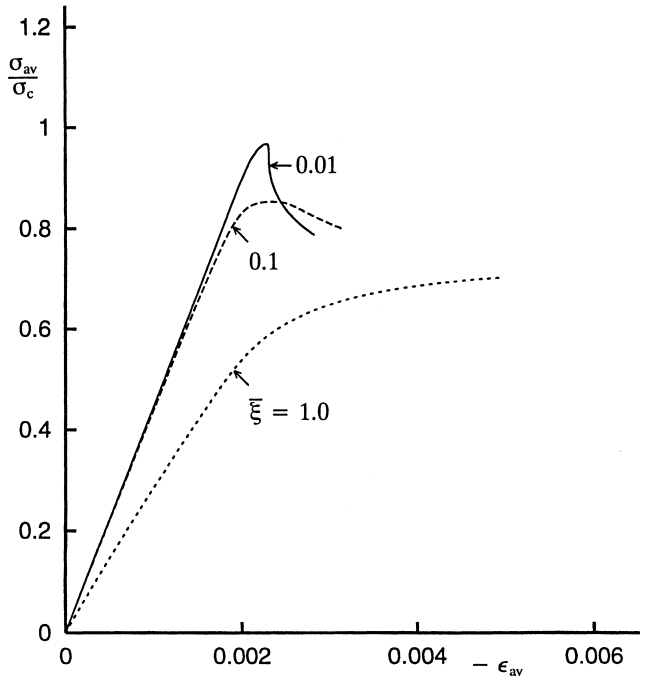

Fig. 5. Average axial stress strain curves for cylindrical panel with $\theta = 0.6$ and $n = 10$, when $\overline{\xi}_1/\overline{\xi} = 0.01$.

To illustrate the behavior, the normal deflections along the center line of a panel, $x^2 = 0$, are shown in Fig. 6 for the smallest imperfection, $\overline{\xi} = 0.01$, corresponding to three different levels of deformation. It is seen that at $\epsilon_{av} = -0.00224$, just before the load maximum, there is not yet any localization, but after the load maximum the buckling deflection grows strongly in a localized region near $x^1 = 0$, while the remaining buckles slowly reduce their amplitude, due to the elastic spring-back under the reduced axial load.

It is noted that, due to the initial imperfections, no bifurcation occurs in the cases illustrated in Fig. 5. However, for a perfect cylindrical panel, bifurcation into a periodic buckling pattern would occur first, and then, after a small amount of growth of the periodic mode, a secondary bifurcation would lead to the onset of buckling localization.

In the next case analyzed, the shell material exhibits more hardening, $n = 3$, and the panel curvature parameter is chosen to be $\theta = 0.75$, but, otherwise, all parameter values are unchanged. For this case, the critical bifurcation stress and the corresponding axial wavelength parameter are $\sigma_c/E = -0.002639$ and $\alpha = 1.056$. For this panel, it has been found (Tvergaard, 1977) that the curvature corresponding to $\theta = 0.75$ is large enough to give an initially unstable post-bifurcation behavior, but that more flat panels show plate-like stable post-bifurcation behavior. The average axial stress vs. strain curves in Fig. 7 show that no maximum is reached for the two larger imperfection amplitudes, whereas the smallest imperfection, $\overline{\xi} = 0.01$, results in a load maximum. The deflections along $x^2 = 0$ in Fig. 8 illustrate the development of a localized buckling pattern after the load maximum for $\overline{\xi} = 0.01$. It is seen by comparing with Fig. 6 that the material with more hardening results in a relatively longer localized region. For the intermediate imperfection amplitude, $\overline{\xi} = 0.01$, where no maximum is reached in Fig. 7, the deflections in Fig. 9 illustrate that the buckles remain periodic. All computations here are carried out using a 24×4 mesh, but it is to be noted

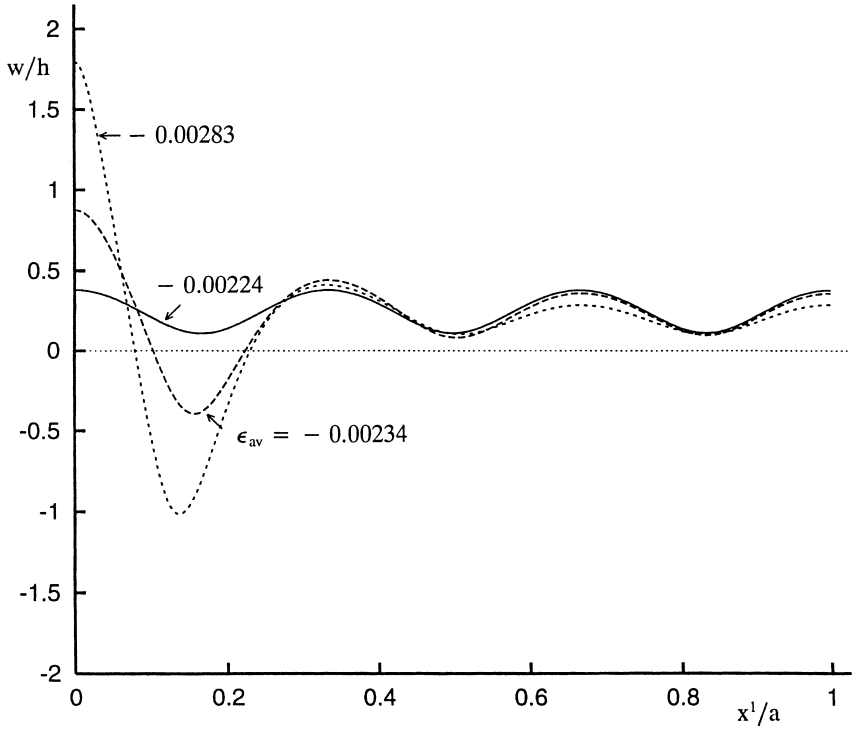

Fig. 6. Normal deflections along the center line, $x^2 = 0$, of cylindrical panel with $\theta = 0.6$, $n = 10$ and $\overline{\xi} = 0.01$, when $\overline{\xi}_1/\overline{\xi} = 0.01$.

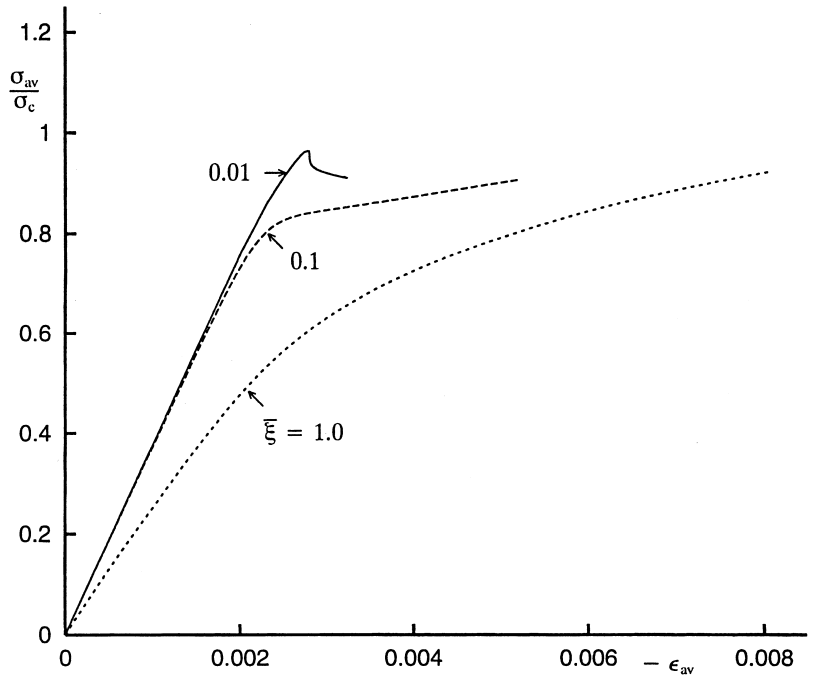

Fig. 7. Average axial stress strain curves for cylindrical panel with $\theta = 0.75$ and $n = 3$, when $\overline{\xi}_1/\overline{\xi} = 0.01$.

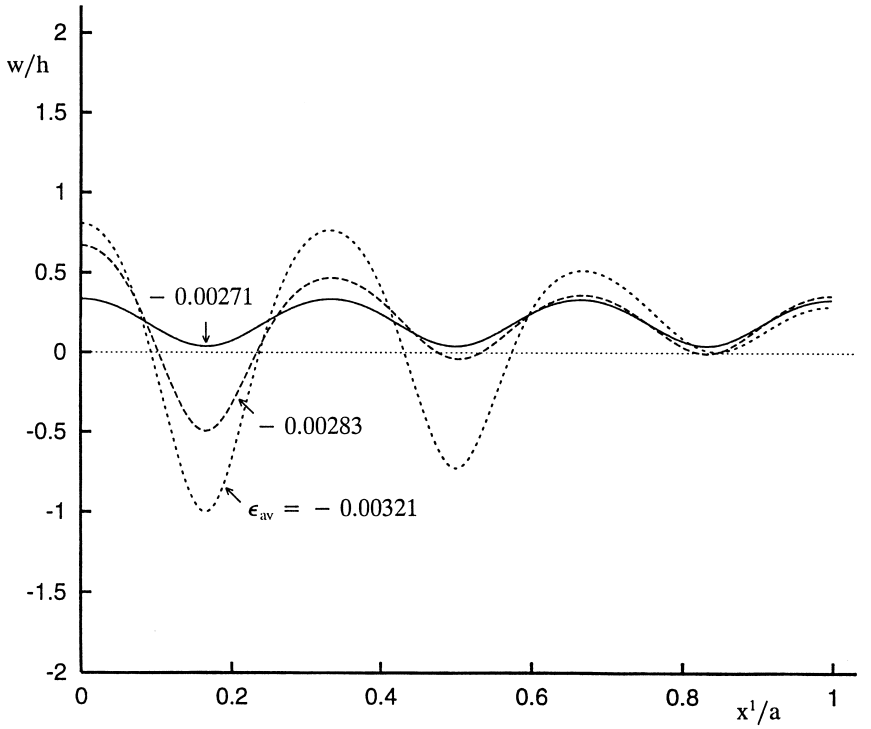

Fig. 8. Normal deflections along the center line, $x^2 = 0$, of cylindrical panel with $\theta = 0.75$, $n = 3$ and $\overline{\xi} = 0.01$, when $\overline{\xi}_1/\overline{\xi} = 0.01$.

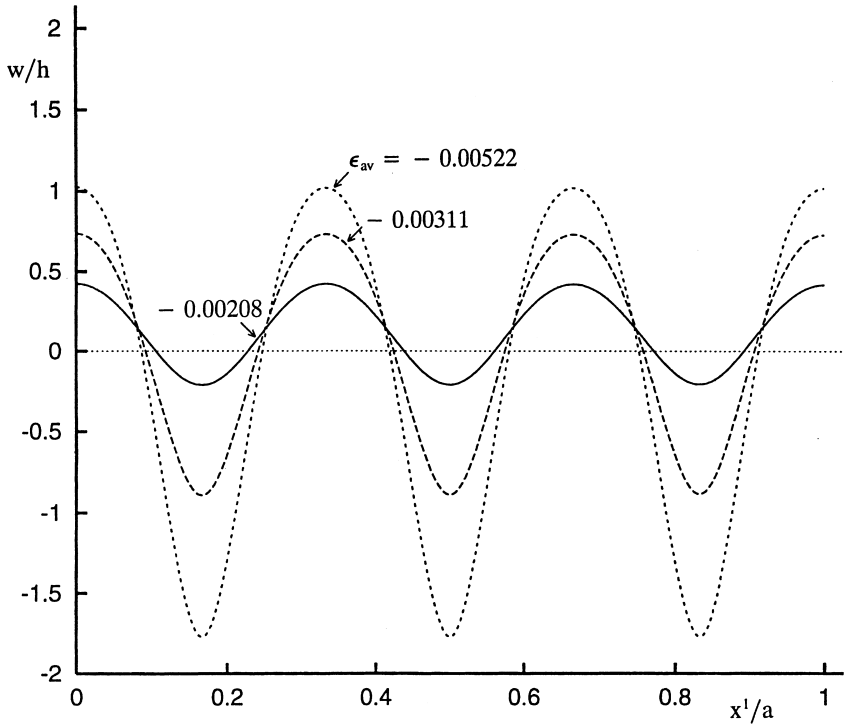

Fig. 9. Normal deflections along the center line, $x^2 = 0$, of cylindrical panel with $\theta = 0.75$, $n = 3$ and $\overline{\xi} = 0.1$, when $\overline{\xi}_1/\overline{\xi} = 0.01$.

that a few computations have been repeated with a finer 36×6 mesh. No mesh dependence has been found, so it can be concluded that the 24×4 mesh gives sufficient accuracy.

For the same panel as that considered in Figs. 7–9, average stress–strain curves are shown in Fig. 10, corresponding to the imperfection amplitude $\overline{\xi} = 0.02$. The solid curve represents material behavior identical to that considered in Figs. 7–9. The lower, dashed curve represents a material that forms a more sharp vertex on the yield surface, as specified by $\phi_0 = \phi_n/2$ and $(\beta_c)_{max} = 135°$. The upper, dotted curve represents a very blunt vertex specified by $\phi_0 = 0°$ and $(\beta_c)_{max} = 91°$, which gives a response essentially identical to that of J_2 flow theory. It is seen in Fig. 10 that a sharper vertex gives a more flexible response, but in fact the three curves are very close, and the main conclusion from Fig. 10 is that the shell does not show much sensitivity to the vertex description in this case. Thus, it can be expected that if all the present localization studies had been based on J_2 flow theory, the predictions would not differ much from those found here.

Fig. 11 shows deflections at $x^2 = 0$ corresponding to the solid curve in Fig. 10. At $\epsilon_{av} = -0.00257$, before the load maximum in Fig. 10, the buckling pattern is still periodic, and then at $\epsilon_{av} = -0.00310$, localization of the buckling pattern has occurred, as would be expected after the load maximum. But subsequently at $\epsilon_{av} = -0.00333$, it is seen that the buckling pattern is again close to periodic. Localization is predicted while the load decays, but the conditions change again when the load starts to increase. In fact, the switch back to a near periodic pattern happens rather abruptly, leaving a small dent on the stress–strain curve, as is clearly seen on all three curves in Fig. 10, near the load minimum. It is noted that this behavior is somewhat analogous to the phenomenon of neck propagation in polymers, where localized necking occurs at a tensile load maximum, but where the material in the neck is subsequently stabilized again as the slope of the stress–strain curve changes from a negative to a positive value.

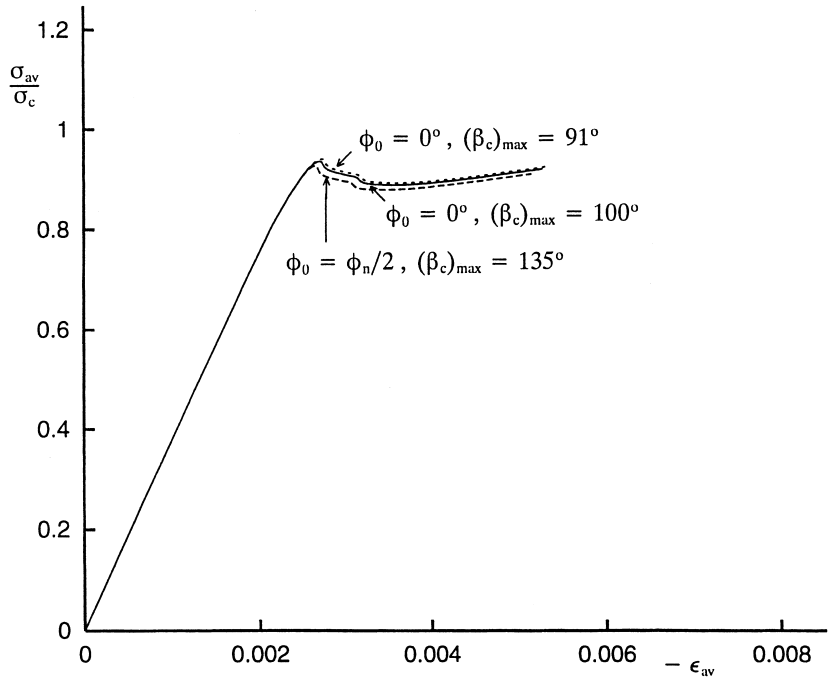

Fig. 10. Average axial stress strain curves for cylindrical panel with $\theta = 0.75$, $n = 3$ and $\overline{\xi} = 0.02$, when $\overline{\xi}_1/\overline{\xi} = 0.01$. The solid curve represent the reference vertex on the yield surface, while the other two curves represent a more sharp vertex and a more blunt vertex.

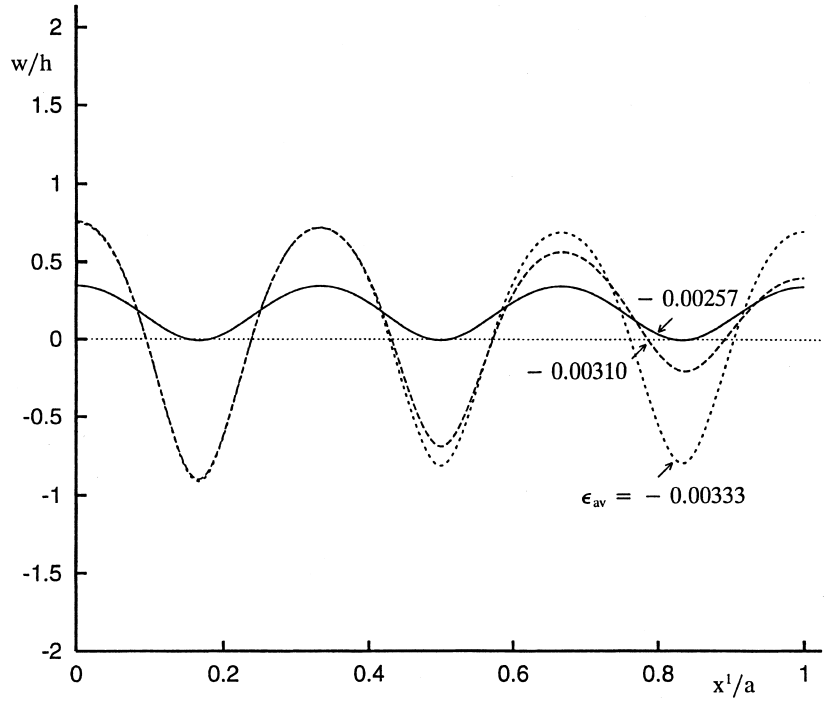

Fig. 11. Normal deflections along the center line, $x^2 = 0$, of cylindrical panel with $\theta = 0.75$, $n = 3$ and $\overline{\xi} = 0.02$, when $\overline{\xi}_1/\overline{\xi} = 0.01$. Corresponds to the solid curve in Fig. 10.

The cases of buckling pattern localization discussed here for cylindrical panels, as well as a number of other cases discussed in Section 2, are associated with elastic–plastic buckling behavior, but naturally conditions for localization would also occur during purely elastic buckling. Therefore, a case of elastic panel buckling is studied in Fig. 12 for $h/b = 0.025$ and $\theta = 0.9$, where the analysis of Koiter (1956) shows unstable initial post-buckling behavior. For $\overline{\xi} = 0.01$ in Fig. 12, the stress–strain curve shows a load maximum, with a subsequent steep load reduction, whereas the curve for $\overline{\xi} = 0.1$ shows no load maximum. For $\overline{\xi} = 0.01$, localization occurs, as illustrated in Fig. 13, in a manner very similar to the results shown in Figs. 6 and 8, but it is to be noted that the numerical value of ϵ_{av} decays during localization, as is also seen just after the load maximum in Fig. 12. For $\overline{\xi} = 0.1$, Fig. 14 shows that no localization develops, as expected.

Computations have also been carried out for very narrow cylindrical panels, with $\theta = 0$ but, otherwise, all parameters chosen are equal to those used in Figs. 5 and 7, respectively. These computations have confirmed the results found by Tvergaard and Needleman (1980) that the lower hardening material shows buckling localization, whereas no load maximum and thus no localization is found for the higher hardening material with $n = 3$.

As buckling localization is also found for some purely elastic cylindrical panels (Figs. 12 and 13), the effect of the nonlinear material behavior may need to be emphasized. As described by the simple model of Section 2.1, localization is predicted if a load maximum occurs, which includes load maxima predicted for purely elastic structures. But material nonlinearity tends to soften the structural response, so that a structure with no maximum in the elastic range may show a maximum in the plastic range, and therefore, the nonlinear material behavior may strongly promote the localization process.

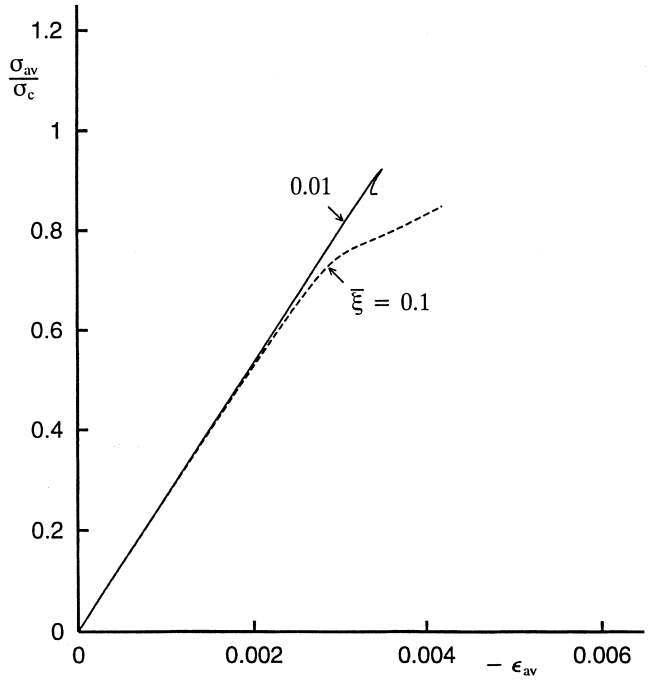

Fig. 12. Average axial stress strain curves for elastic cylindrical panel with $\theta = 0.9$, when $\overline{\xi}_1/\overline{\xi} = 0.01$.

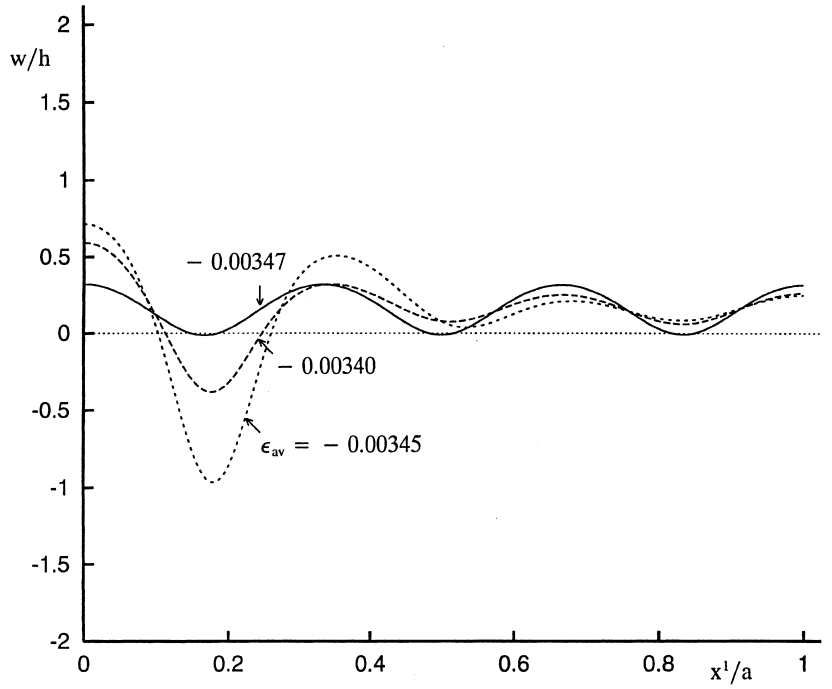

Fig. 13. Normal deflections along the center line, $x^2 = 0$, of elastic cylindrical panel with $\theta = 0.9$ and $\overline{\xi} = 0.01$, when $\overline{\xi}_1/\overline{\xi} = 0.01$.

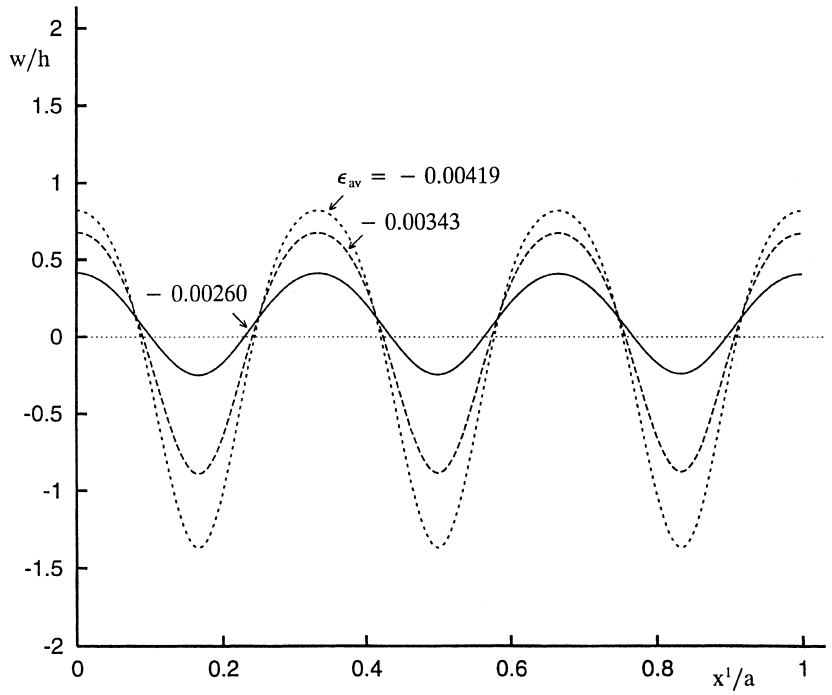

Fig. 14. Normal deflections along the center line, $x^2 = 0$, of elastic cylindrical panel with $\theta = 0.9$ and $\overline{\xi} = 0.1$, when $\overline{\xi}_1/\overline{\xi} = 0.01$.

References

Batdorf, S.B., 1949. Theories of plastic buckling. J. Aeronaut. Sci. 16, 405–408.
Christoffersen, J., Hutchinson, J.W., 1979. A class of phenomenological corner theories of plasticity. J. Mech. Phys. Solids 27, 465–487.
Considere, M., 1885. L'Emploi du fer et de l'acier dans les constructions. Annales des Ponts et Chaussées 9, 574–775.
Gellin, S., 1979. Effect of an axisymmetric imperfection on the plastic buckling of an axially compressed cylindrical shell. ASME J. Appl. Mech. 46, 125–131.
Hutchinson, J.W., 1974. Plastic buckling. Adv. Appl. Mech. 14, 67–144.
Hutchinson, J.W., Miles, J.W., 1974. Bifurcation analysis of the onset of necking in an elastic–plastic cylinder under uniaxial tension. J. Mech. Phys. Solids 22, 61–77.
Ju, G.T., Kyriakides, S., 1992. Bifurcation and localization instabilities in cylindrical shells under bending – II. predictions. Int. J. Solids Struct. 29, 1143–1171.
Koiter, W.T., 1945. Over de stabiliteit van het elastisch evenwicht., Thesis, Delft, H.J., Paris, Amsterdam. English translations (a) NASA TT–F10, 1967; (b) AFFDL–TR–70-25, 1970.
Koiter, W.T., 1956. Buckling and post–buckling behaviour of a cylindrical panel under uniaxial compression. National Luchtvaart Laboratorium, 20, Report S476, Amsterdam.
Koiter, W.T., 1966. On the nonlinear theory of thin elastic shells. Proc. Kon. Ned. Ak. Wet. B69, 1–54.
Kyriakides, S., Ju, G.T., 1992. Bifurcation and localization instabilities in cylindrical shells under bending – I experiments. Int. J. Solids Struct. 29, 1117–1142.
Mikkelsen, L.P., 1995. Elastic–viscoplastic buckling of circular cylindrical shells under axial compression. Eur. J. Mech. A/Solids 14, 901–920.
Moxham, K.E., 1971. Buckling tests on individual welded steel plates in compression. Cambridge University Engineering Department, Report CUED/C-Struct/TR.3.
Needleman, A., 1988. Material rate dependence and mesh sensitivity in localization problems. Comp. Meth. Appl. Mech. Engng. 67, 69–85.
Needleman, A., Tvergaard, V., 1982. Aspects of plastic post-buckling behavior. In: Hopkins, H.G., Sewell, M.J. (Eds.), Mechanics of Solids. The Rodney Hill Sixteth Anniversary Volume. Pergamon Press, New York, pp. 453–498.
Niordson, F.I., 1985. Shell Theory. North-Holland series Appl. Math. Mech. Vol. 29.
Tvergaard, V., 1976. Effect of thickness inhomogeneities in internally pressurized elastic–plastic spherical shells. J. Mech. Phys. Solids 24, 291–304.
Tvergaard, V., 1977. Buckling of elastic–plastic cylindrical panel under axial compression. Int. J. Solids Struct. 13, 957–970.
Tvergaard, V., 1983a. Plastic buckling of axially compressed cylindrical shells. Int. J. Thin–Walled Struct. 1, 139–163.
Tvergaard, V., 1983b. On the transition from a diamond mode to an axisymmetric mode of collapse in cylindrical shells. Int. J. Solids Struct. 19, 845–856.
Tvergaard, V., Needleman, A., 1980. On the localization of buckling patterns. ASME J. Appl. Mech. 47, 613–619.
Tvergaard, V., Needleman, A., 1981. On localized thermal track buckling. Int. J. Mech. Sci. 23, 577–587.
Tvergaard, V., Needleman, A., 1983. On the development of localized buckling patterns. In: Thompson, J.M.T., Hunt, G.W. (Eds.), Collapse: The Buckling of Structures in Theory and Practice. Cambridge University Press, London, pp. 1–17.